View Online / Journal Homepage
Dynamic Article Links

Soft Matter

Cite this: DOI: 10.1039/c2sm00024e

www.rsc.org/softmatter

PAPER

Pathway switching in templated virus-like particle assembly

Irina Tsvetkova,[a] Chao Chen,[a] Subinoy Rana,[c] C. Cheng Kao,[b] Vincent M. Rotello[c] and Bogdan Dragnea*[a]

Received 4th January 2012, Accepted 21st February 2012
DOI: 10.1039/c2sm00024e

Assembly pathways of virus-like particles formed from a virus coat protein cage encapsulating a metal nanoparticle were studied by intrinsic fluorescence quenching. Depending on buffer conditions, the *in vitro* formation of a virus-like particle can take place through cooperative or non-cooperative adsorption of protein subunits on the nanoparticle template. Simple equilibrium models provided estimates for the thermodynamic forces driving the assembly as well as the size of the critical nucleus in the case of cooperative growth.

Introduction

Among myriad examples of molecular self-organization under study today, virus assembly stands out owing to several unique characteristics. For instance, while deterministic molecular structure is traditionally associated with covalent or ionic bonding, many viruses represent supramolecular structures which are built with the same stoichiometric precision as small molecules but from hundreds to thousands of proteins which are held together by comparatively weak, non-covalent interactions. Thus, protein cages encapsulating viral genomes such as the capsids of many single-stranded (ss) DNA and RNA viruses, and the cores of many enveloped viruses are based on geometrical arrangements of a fixed number of protein subunits[1] and numerous examples exist in which same structures form *in vitro*, by spontaneous assembly from purified components.[2–4]

Furthermore, symmetric viral architectures can be highly dynamic, being capable of large global structural transformations in response to environmental cues. Some of these transformations are irreversible, corresponding to different stages in the virus life cycle. Reversible global structural transitions also exist, *e.g.* the swelling transition characteristic of plant viruses in the *Bromoviridae* family.[5]

The view of the general driving forces behind virus self-assembly has remained largely unaltered since the beginning of studies of the construction of regular viruses: under appropriate solvent conditions, nucleic acid and protein subunits spontaneously come together to form a virus particle because this is their lowest free energy state which corresponds to the maximum number of the most stable bonds between subunits.[6–8] However, for even the simplest viruses, the pathways of transition from a state in which protein subunits and nucleic acid are randomly distributed to a state in which they are highly ordered remain unclear.

For a few simple viral cages sharing the feature of an icosahedral arrangement of identical proteins, significant insight into assembly mechanisms came from *in vitro* kinetic studies of association reactions between capsid proteins alone.[9–11] Kinetic features of assembly suggested that the process occurs through directed, highly cooperative, nucleated reactions. In such cases, the nature of the nucleus for assembly could be inferred from the assembly half-life that depends on capsid protein concentration.[12]

While empty capsid formation studies were crucial for understanding subunit–subunit interactions, their relevance in terms of mechanisms for actual virus assembly has been questioned.[13] The argument was based upon the fact that empty capsid can form in a sequential, cooperative manner, by addition of subunits to the edge of an incomplete capsid. However, in presence of nucleic acid, self-assembly of protein subunits into the geometric shells of polyhedral viruses has been proposed to proceed by condensation of nucleic acid complexed with the amino terminal polypeptides of the coat proteins, in a manner similar to micelle formation.[13] In this case, as a result of condensation, crowding of capsid proteins excludes further monomer addition and the entire nucleo–protein complex collapses into its ground state. Currently, it is not clear whether the sequential mechanism continues to play a role in native virus formation. In other words, it is not known whether the two mechanisms, "sequential" and "micelle-like", are exclusive.

The discovery that some icosahedral ssRNA plant virus capsids can assemble in their native structures around non-genomic templates such as foreign nucleic acids,[4] polymers,[14,15] enzymes,[16] nucleic-acid functionalized particles,[17,18] and other ligand-coated particles[19–22] opened the way of tuning the interaction between the encapsulated material and the protein capsid and thus probing the role of this interaction in assembly.

In this paper, a ligand-coated nanoparticle template approach was taken which allowed equilibrium studies of the intrinsic

[a]*Department of Chemistry, Indiana University, Bloomington, IN 47405, USA. E-mail: dragnea@indiana.edu; Tel: +812-856-0087*
[b]*Department of Biology, Indiana University, Bloomington, IN 47405, USA*
[c]*Department of Chemistry, University of Massachusetts, Amherst, MA 01003, USA*

protein fluorescence quenching as a function of protein/core ratio.

The results indicate that, in presence of a polyanionic nanoparticle (NP) acting as a mimic for the nucleic acid core, template-directed assembly of brome mosaic virus (BMV) capsid proteins can switch between qualitatively different growth mechanisms. More specifically, in conditions of high pH and low ionic strength initial random association of the protein with the anionic core occurs that can be modelled by simple Langmuir adsorption. However, in conditions of low pH and low ionic strength that are conducive for *in vivo* assembly of infectious virions, the initial protein-core association is followed by a step in which template-bound proteins rearrange in a regular capsid structure. In this case, assembly is cooperative and a critical amount of template-bound protein is required for efficient capsid growth.

Results

Brome Mosaic virus (BMV) is a well-studied, simple ssRNA plant virus having a tripartite genome encapsulated in a T = 3 capsid formed from 180 copies of the same capsid protein.[23] BMV capsid proteins spontaneously assemble around non-genomic templates in place of the native nucleic acid, *e.g.* gold nanoparticles functionalized with carboxylate-terminated thiolalkylated tetraethylene glycol ligand (GNP) (Fig. 1).[19] Virus-like particles (VLPs) encapsulating 12 nm diameter particle cores exhibit the structural characteristics of a T = 3 array, similar to the native structure.[24] Moreover, VLPs will co-crystallize with native viruses in any proportion and will exhibit a swelling transition in same conditions as the native virus.[19,24] Template-capsid protein interactions are dominated by electrostatic forces, which also make an important component of the native RNA–capsid protein (CP) interaction.[14] Thus, in view of similarities between VLPs and BMV, the assembly of capsid proteins around functionalized nanoparticle cores represents an experimental model for virus assembly situated between empty capsid and native virus assembly. Nanoparticle-templated assembly is more amenable to modelling than full virus assembly due to a reduced number of parameters driving the process.[25–27] Moreover, access to real-time measurements down to the single VLP scale is facilitated by the nanoparticle optical properties.[28]

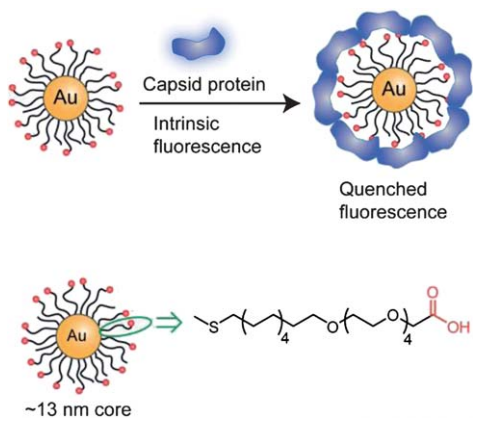

Fig. 1 Schematic representation of GNP functionalized with carboxylate-terminated thiolalkylated tetraethylene glycol ligand (lower) and protein capsid assembly around GNP.

The protein subunits of small icosahedral plant viruses such as BMV self-assemble *in vitro* into a plethora of polymorphs depending on concentration, pH and ionic strength conditions.[29,30] Such maps of pH and ionic strength ranges corresponding to stable conformations at equilibrium are termed "phase diagrams" by analogy with the phase equilibria in bulk systems, Fig. 2(a). Phase diagrams have not yet been reported for any nanoparticle-templated protein cage system. However, it is known that VLPs formed from 12 nm diameter gold nanoparticles coated with short carboxylated polyethylene glycol chains yield stable structures of similar morphology with native viruses at low pH and ionic strength, Fig. 2(a)[19] and unstable at high pH and high ionic strength. In terms of assembly efficiency, kinetics may differentiate between possible phase diagram pathways connecting the disassembled free components and the VLP state. A pathway commonly used for efficient nanoparticle encapsulation is sketched in Fig. 2(a). Insight into the mechanism of nanoparticle packaging along a particular pathway can be gained by measuring the relative amount of template bound protein as a function of protein/core molar ratio. For example, by titrating viral RNA with capsid protein and measuring native gel electrophoretic displacement, Johnson *et al.* have shown that the CP binds RNA and slowly folds into a compact quaternary structure which then supports highly cooperative assembly.[32]

Measurements based upon mobility in a viscous medium such as electrophoresis or dynamic light scattering are challenged by the fact that the hydrodynamic diameter is affected not only by stoichiometry but also by shape. Moreover, when mobility is determined from motion in an electric field, the question arises whether the native electrostatic interactions holding the system together could be offset by the external field. This is especially true for complexes at low protein/core ratios which are expected to correspond to far from spherical geometries and held together by weak, non-covalent bonds. Nevertheless, such methods have been widely used in the study of virus assembly because of their

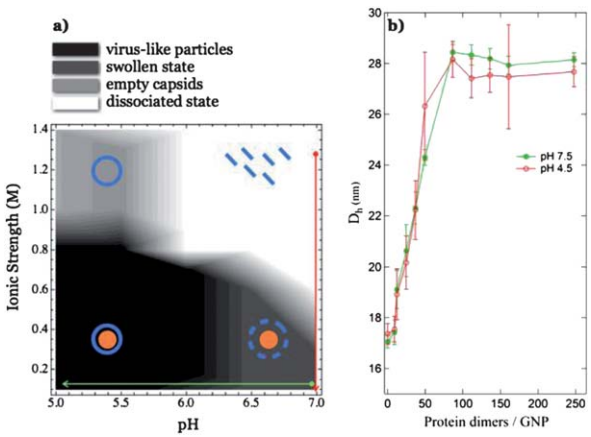

Fig. 2 (a) Phase diagram representation of reconstituted BMV (adapted from ref. 31) overlaid with symbols representing the stable states of VLP constituents. The red and green arrows represent the two successive pathways discussed in this paper. (b) DLS-measured hydrodynamic diameters for states corresponding to different CP/GNP ratios at neutral and acidic pH.

compatibility with physiological conditions and lack of labelling requirements. Fig. 2(b) shows an example of DLS measurements of the average hydrodynamic diameter as a function of the CP/GNP ratio. It is clear that DLS can qualitatively follow titration of GNPs by protein and it shows that a stationary state is reached at ~90 dimers per GNP, which corresponds to a complete coverage assuming the formation of a T = 3 particle. Moreover, the average maximum diameter attained at neutral pH is 28.4 nm, while the value corresponding to acidic pH is smaller, 27.3 nm. This difference is probably due to swelling at close-to neutral pH, characteristic for *Bromoviridae*.[5] However, at low CP/GNPs ratios, there are no differences detectable by DLS between acidic and neutral conditions.

To monitor VLP formation by a method that probes the amount of protein adsorbing on the NP surface more directly, we have used native fluorescence quenching by GNPs[33] at same titration conditions as those in the DLS experiments in Fig. 2. Upon excitation by UV light (~290 nm wavelength), intrinsic protein fluorescence at 330–360 nm arises from aromatic residues such as tryptophan, tyrosine, and phenylalanine. Fluorescence is generally quenched upon protein adsorption at the GNP surface. This is due to an increase in the non-radiative relaxation rate in the vicinity of the metal as well as a decrease in the radiative rate at 2–3 nm from the metal surface.[34] In a first approximation, the change in fluorescence intensity is directly proportional with the amount of protein adsorbed on GNP cores.

Fluorescence titration results for the neutral pH step (pH 7.5) are plotted in Fig. 3 *vs.* total protein dimer–GNP molar ratio, along with a pure protein control. For the control (only protein, no GNPs), the dependence of fluorescence intensity on protein concentration is linear for a dilute solution. In the case of the CP/GNP mixture, the fluorescence intensity dependence on the CP dimer to GNP ratio is clearly biphasic, with a break point below 100 CP dimers per GNP. The CP/GNP mixture data is fitted satisfactorily by a Langmuir adsorption model which provides an estimate of the dissociation constant K_d and of the number of CP dimers per VLP at surface saturation. The model is described in detail in the discussion section.

At pH 4.5, the fluorescence binding assay exhibited a different character than at pH 7.5, Fig. 4. At low CP:GNP ratio (less than ~15 dimers per GNP) an initial fast rise occurred, characterized by a slope parallel to that of pure protein control. At ratios greater than ~15 CP dimers/GNP, an intermediate zone of slower increase of fluorescence with added relative amount of protein was observed. This intermediate phase lasted up to ~110 CP dimers/GNP, at which point the onset of a third phase of slope parallel to the pure protein control data was observed. The efficiency of incorporation, calculated as a ratio of GNPs incorporated into full capsids to the total amount of GNPs from TEM images, was around 80%, which is consistent with previous results for VLP assembly.[19] As discussed later, a Hill model simulation for cooperative binding reproduced well the multi-phasic behavior observed and allowed for an estimate of the dissociation constant.

Analysis of negatively stained TEM micrographs showed small differences in the average diameter but marked differences in the morphology of assembly results corresponding to the two conditions discussed in this paper, Fig. 5. Thus, VLP diameter was 31 ± 3 nm at pH 7.5 and 28 ± 2 nm at pH 4.5.

Centered and azimuthally averaged micrographs of VLPs at pH 4.5 and pH 7.5 are presented in Fig. 6. Structural details are clearly more marked at pH 4.5. From the gold surface outwards, one can

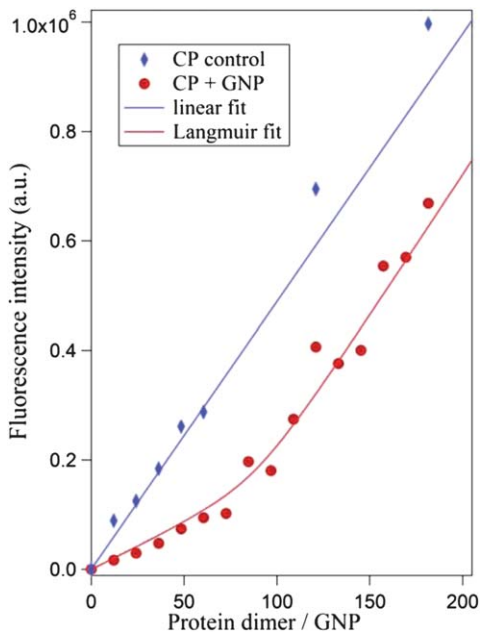

Fig. 3 Fluorescence intensity as a function of the ratio of CP dimer to GNP (red dots) at pH 7.5 and pure CP control (blue diamonds). The red line represents a Langmuir adsorption fit to the CP/GNP mixture data (p-value < 0.05) and the blue line represents a linear fit to the pure protein control.

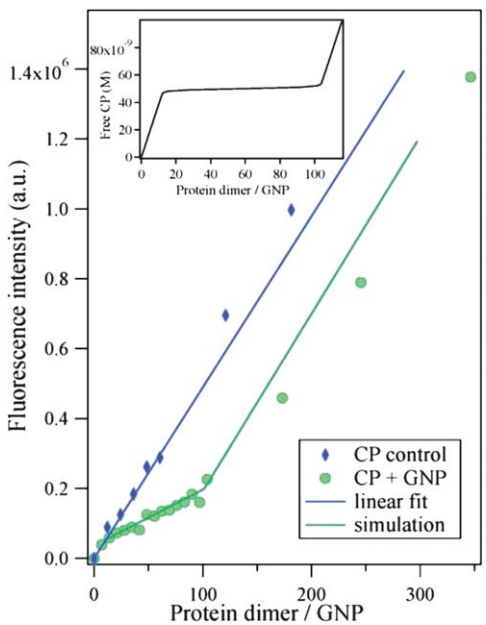

Fig. 4 Fluorescence intensity as a function of the ratio of CP dimer to GNP (green dots) at pH 4.5 and pure CP control (blue diamonds). The line represents a cooperative binding simulation based upon the Hill model (p-value < 0.05). Inset: free CP concentration as a function of total CP:Au ratio according the model.

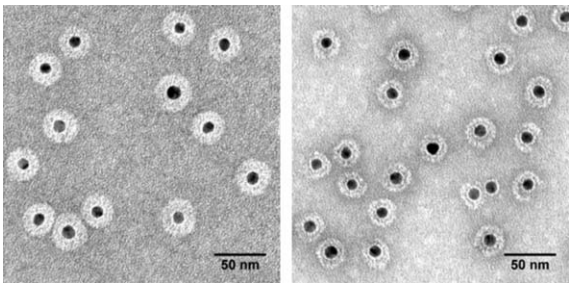

Fig. 5 TEM micrographs of VLPs at pH 7.5 (left) and pH 4.5.

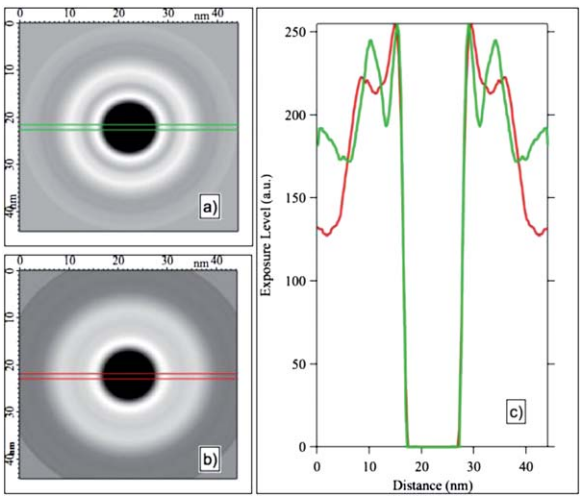

Fig. 6 Averages of VLP TEM pictures showing differences in the radial distribution of the coat material. (a) VLPs at pH 4.5, (b) VLPs at 7.5, (c) cross-sectional radial gray level intensity distribution for data in (a) and (b).

observe first a bright shell peaking at ~1.8 nm from the Au surface. This is probably due to the dense TEG layer. A darker ring follows at ~4.2 nm. This is a region of negative stain accumulation, mostly occupied by solvent. After this region of dense staining, a ring of low stain density appearing bright in the image follows with a peak at 7.5 nm from the Au surface. The breadth of this outer ring is ~4.2 nm. These dimensions correspond well to the expected radial extent of hydrophobic capsomeric contacts in the capsid.[23] By contrast with the well-defined radial structure observed at pH 4.5, a much shallower gap can be observed at pH 7.5 between the capsid and the ligand layer. In general, at neutral pH, all observable features are much less prominent.

Discussion

At pH 7.5, 99% of carboxyl groups on the nanoparticle surface are ionized[35,36] and the GNP surface interacts attractively with basic free protein dimer termini. The first phase in the titration curve at pH 7.5 thus corresponds to binding of free protein to GNPs and is characterized by a slow rate of fluorescence increase with the CP concentration. The second phase corresponds to saturation of surface sites by protein. As a consequence, further addition of CP results in the same rate of fluorescence increase as observed for pure CP, Fig. 3.

The process is described by the reaction:

$$CPD_{free} + S^{*} \rightleftarrows CPD_{bound} \quad (1)$$

where CPD_{free} = free capsid protein dimer, S^{*} = empty surface sites, CPD_{bound} = bound protein dimer (equivalent with occupied surface sites).

Note that other reactions involving protein oligomerization will contribute a negligible amount to the signal since they are not accompanied by fluorescence quenching. The dissociation constant corresponding to reaction eqn (1), K_d, is:

$$K_d = \frac{(1-\theta)\left[CPD_{free}\right]}{\theta} \quad (2)$$

where θ represents the fractional GNP surface coverage:

$$\theta = \frac{\left[CPD_{free}\right]_0 - \left[CPD_{free}\right]}{[S]_0} \quad (3)$$

and $[S]_0$ and $[CPD_{free}]_0$ are the initial concentration of empty surface sites and free protein dimer, respectively. Thus, eqn (1)–(3) summarize the protein–nanoparticle association in terms of a simple Langmuir adsorption model.[37]

$[S]_0$ in eqn (3) is found from:

$$[S]_0 = n \times [GNP]_0 \quad (4)$$

where n is the number of CP dimers corresponding to the saturation coverage of one GNP (*e.g.* for a T = 3 capsid: $n = 90$). The gold nanoparticle concentration in all experiments was maintained at $[GNP]_0 = 3.86$ nM.

Substituting (4) in (3) gives:

$$\theta = \frac{1}{n}\left(r - \frac{\left[CPD_{free}\right]}{[GNP]_0}\right) \quad (5)$$

where r is the molar ratio of capsid protein dimer to gold, *i.e.* the independent variable of all titration experiments.

By substituting $[CPD_{free}]$ from (5) into (2), the following quadratic equation in θ is obtained:

$$n\cdot\theta^2 - (r + n + K_d/[GNP]_0)\cdot\theta + r = 0 \quad (6)$$

Eqn (6) has two real roots, but only one is physically acceptable based upon the expectation that $\theta = 0$ when $r = 0$:

$$\theta(r) = \frac{r + n + K_d\Big/[GNP]_0 - \sqrt{\left(r + n + K_d\Big/[GNP]_0\right)^2 - 4n\cdot r}}{2n} \quad (7)$$

Expression (7) provides the basis for generating the fit function for the fluorescence intensity curve as a function of r in Fig. 2. Thus, total fluorescence intensity, $I_F(r)$, is the result of two contributions: the first coming from free protein in solution and the second from surface-bound protein:

$$I_F(r) = a\cdot[r - n\cdot\theta(r)] + b\cdot n\cdot\theta(r) \quad (8)$$

where the a and b coefficients stand for the rates of fluorescence change corresponding to free and bound protein, respectively. Their values were determined experimentally from the

corresponding slopes of the linear regimes in Fig. 2. Expression (8) thus provided a fitting function with two parameters: n and K_d. Parameter values yielding the least square fitting of experimental data in Fig. 2 were n = 90 (which corresponds to a T = 3 protein cage) and $K_d = 1.2 \pm 1.1$ nM. Due to the substantial fit uncertainty in the dissociation constant value, one can only infer from the data an upper limit for K_d at approx. 2 nM. The Gibbs free energy of reaction per CP dimer corresponding to this K_d value is:

$$\Delta G^{pH7.5}_{dimer} = -RTln(K_d) \approx -12 \text{ kcal mol}^{-1} \quad (9)$$

The observed lack of cooperativity at neutral pH implies that the process must rely mainly on the attractive electrostatic interactions between core and the CP N-termini and that protein-protein interactions may be a minor factor in this case. This could explain why we do not see a similar degree of ordering in the shell at pH 7.5 as we see at pH 4.5, Fig. 5. Interestingly, the n value found from the fit is the same with the number of dimers in a T = 3 capsid, which suggests that a close-to correct number of subunits for a T = 3 may be already pre-assembled at this step.

At pH 4.5, 20–40% of carboxyl groups on the nanoparticle surface are ionized[35,36] and the attractive electrostatic component of the interaction between the nanoparticle and the protein is drastically decreased. At low CP:GNP ratio, the high cost in translational entropy of recruiting CPs and assembling them into a VLP probably outweighs the energetic advantage of core–protein electrostatic interactions, now weakened. Therefore, in this case the solution mainly contains CP dimers (and mostly bare GNPs); addition of CP merely results in an increase of the free protein in solution as indicated by the first phase in Fig. 4 having approximately the same slope as the pure CP control.

At high concentrations, there is less translational entropy to overcome. The binding energy dominates and CP gets assembled into VLPs. In this regime, a fraction of the newly added protein ends up on the GNP surface, which quenches its fluorescence, hence the different slope of the second phase.

Finally, once all GNP surface adsorption sites have been occupied, further addition of CP to solution will solely result in increasing the amount of free protein and thus the fluorescence rate will approach the pure CP control, once again.

The overall sigmoidal shape and relatively sharp transitions between these regimes suggest cooperative binding. This can be formally illustrated by applying a Hill model to the problem and assume that exactly n CPs could bind to a GNP:[38]

$$CP + \frac{1}{n} \cdot GNP \mapsto \frac{1}{n} VLP \quad (10)$$

Then, the VLP concentration can be written as a function of the dissociation constant K:

$$[VLP] = \frac{[GNP]_0}{1 + \left(\frac{K}{[CPD_{Free}]}\right)^n} \quad (11)$$

And the relationship between the CP:GNP ratio, r, and the concentration of free protein becomes:

$$r = \frac{[CPD_{Free}]}{[GNP]_0} + \frac{n}{1 + \left(\frac{K}{[CPD_{Free}]}\right)^n} \quad (12)$$

At the same time, eqn (8) for the fluorescence intensity as a function of CP:Au ratio can be re-written as:

$$I_F = a \cdot \frac{[CPD_{Free}]}{[GNP]_0} + b \cdot \frac{n}{1 + \left(\frac{K}{[CPD_{Free}]}\right)^n} \quad (13)$$

where a and b are the same numerical coefficients as those of data in Fig. 2, and n are fit parameters, with n corresponding to the Hill exponent. Since the free CP concentration cannot be easily extracted from (12) and substituted in (13) to provide an analytical expression for $I_F(r)$, we have opted to calculate I_F in the form of an implicit representation (simultaneously utilizing (12) and (13) with $[CPD_{Free}]$ as the independent variable). Satisfactory agreement between simulation and experiment is achieved for $n = 90$, which corresponds to a $T = 3$ capsid, and $K = 42$ nM. Therefore, the Gibbs free energy of reaction is approximately:

$$\Delta G^{pH4.5}_{dimer} = -RTln(K_d) \approx -10 \text{ kcal mol}^{-1} \quad (14)$$

The model allows us to examine the relationship between free protein in solution and the total CP:Au ratio (inset of Fig. 3). Thus, the onset of efficient adsorption, which marks the passage from nucleation to elongation, only occurs after 12 ± 3 dimers have been already adsorbed on the GNP surface. Interestingly, Johnson *et al.* have studied by electrophoresis the *in vitro* assembly of the chlorotic cowpea mottle virus (CCMV), a close relative of BMV, and have found that, at near to physiological conditions, the elongation phase was triggered by the formation of a nucleoprotein complex containing approximately ten CCMV dimers per RNA1.[32] In contrast, analysis of assembly kinetics for empty CCMV particles suggested that the elongation phase begins with the formation of pentamers of dimers.[11] We conclude that in the case of VLP assembly, the onset of the elongation phase is more similar to viruses than to empty capsids. At this point, however, it remains unclear why 10–12 dimers (and not 5) are involved in the nucleation step.

As the inset of Fig. 3 suggests it, the elongation phase is astonishingly efficient: almost every newly added CP dimer will be recruited by a growing capsid. However, cooperativity at this level is not a rare occurrence in biological systems, since ultra-sensitivity to ligand concentrations is often an important characteristic of biological regulation.[39]

The previously reported thermodynamics of empty capsid assembly, in combination with the currently reported data, also provide a way to evaluate the weight of different contributions to the thermodynamic driving force behind assembly. Thus, empty CCMV capsid assembly is characterized by a critical concentration corresponding to an apparent K_d of 2 μM at pH 4.8.[40] The Gibbs free energy of reaction is $\Delta G = (89/90)$ RT $\ln(K_d) = -7.5$ kcal mol^{-1}. This is about 75% of the value found for VLPs at pH 4.5. Therefore, at acidic pH, VLP assembly is dominated by protein-protein interactions. Since this is also the case with empty capsids and since empty capsid assembly is highly cooperative,[11] it is not surprising that the same cooperativity is

observed for VLPs. However, the size of the critical nucleus is different for VLPs and empty capsids. It would be of interest to elucidate the origins of this difference and the structure(s) associated with it.

Methods

BMV protein preparation

Capsid subunits were obtained from BMV particles purified from infected plants as described in ref. 41. To separate capsid subunits from BMV RNA, 100 μl of intact BMV (2 mg ml^{-1}) were dialyzed against a solution containing 0.5 M $CaCl_2$ solution at 4 °C for 24 h. The insoluble material containing viral RNA was removed by centrifugation at 16 000 g for 40 min at 4 °C. The supernatant containing the dissociated proteins was then dialyzed against 0.01 M Tris base, pH 7.4 for 24 h at 4 °C to remove residual calcium ions and then dialyzed against buffer of 0.01 M Tris base, 1 M KCl, 0.005 M MgCl2 and pH 7.4 for 24 h at 4 °C. The integrity of the capsid subunits was confirmed by matrix-assisted laser desorption/ionization time-of-flight mass spectrometry. Before the experiments, dissociated proteins were dialyzed overnight against buffer A at pH 7.5 and low ionic strength (0.05 M Tris-HCl, 0.05 M NaCl, 0.01 M KCl, 0.005 M $MgCl_2$). Protein concentration was determined by UV-vis spectrometry.

Au nanoparticle preparation

TEG-coated Au particles were synthesized according to a previously described procedure.[19] Particle size was measured to be 11.1 ± 0.9 nm by TEM. TEG-coated Au particles were dialyzed against a buffer A of low ionic strength and pH 7.5 for 24 h before the experiment. The number density of Au particles was calculated based on absorbance at 400 nm and the known dependence of the extinction cross-section on particle size.

Dynamic light scattering

Dynamic light scattering (DLS) measurements were carried out with a Zetasizer NanoS (Malvern Instruments). For experiments at neutral pH, 25 μl of 20 nM Au-TEG in the buffer of 0.05M Tris-HCl, 0.05M NaCl, 0.01M KCl, 0.005M $MgCl_2$ at pH 7.5 were mixed at room temperature with various amount of protein (2–75 μl of 5.6 μM protein dimer) as well as compensatory amounts of buffer to make a summed volume of 100 μl.

For the titration assay at pH 4.5, samples from a similar assembly series as above were each mixed with 0.05M NaOAc, 0.008M $Mg(OAc)_2$ buffer at pH 4.0 at a ratio of 3: 1. Measurement duration was set to be determined automatically, and data were averaged from at least three runs. Intensity and volume distributions of the particle sizes were recorded.

Fluorescence binding assay

For the neutral pH experiment, 50 μl of 20 nM Au-TEG in the buffer of 0.05M Tris-HCl, 0.05M NaCl, 0.01M KCl, 0.005M $MgCl_2$ and pH 7.5 were mixed at room temperature with various amounts of protein (2–150 μl of 5.6 μM protein dimer in the same buffer) as well as compensatory amounts of buffer to make a total volume of 200 μl. However, the actual final volume was generally different than the expected value from summation. Nevertheless, small adjustments were done to compensate for the error by measuring the total Au concentration light absorbance and adjusting the volume to maintain it at 3.86 nM.

Fluorescence collected at an angle of 90 degrees from the assembly mixture was then measured at room temperature for an excitation wavelength of 280 nm and an emission wavelength of 340 nm (SPEX Fluoromax 2 fluorimeter, Instruments SA, Inc., Edison, NJ). A series of control samples, which contained the same components as the assembly series except for Au, were also measured. For data analysis, fluorescence from the assembly series had to be corrected due to the Au absorbance at the excitation and the emission wavelengths. The correction was made according to the formula:[42]

$$lg\frac{F_{correct}}{F_{observed}} = \frac{A(emission) + A(excitation)}{2}$$

where F denotes fluorescence intensity and A represents the Au absorbance. Absorbance measurements of Au at the concentration of $[Au]_0$ resulted in: $F_{correct} = 1.5 \times F_{observed}$.

To perform the fluorescence binding assay at pH 4.5, the assembly series from above were each mixed with a buffer of 0.05M NaOAc, 0.008M $Mg(OAc)_2$ at pH 4.0 at the ratio of 3 to 1. Again, the actual final concentrations had to be determined experimentally and we found $[Au]_0 = 2.05$ nM in this case. In order to compare these results to those obtained from neutral pH condition, they have to be multiplied by an absorbance factor of 1.23 and a dilution factor, 3.86/2.05 = 1.88, *i.e.*, in this case: $F_{corrected} = 1.23 \times 1.88 \times F_{observed}$.

Conclusions

An intrinsic *in vitro* fluorescence quenching assay was developed to examine the self assembly process of nanoparticle-templated virus-like particles derived from BMV, at near to physiological conditions. At neutral pH, non-cooperative association of capsid proteins with the nanoparticle template occurred which was described by a Langmuir adsorption model. At acidic pH, the assembly is highly cooperative requiring the formation of a critical nucleus of proteins adsorbed on the particle surface. The size of the nucleus in this case is 2–3 times larger than that previously observed for empty capsid formation. These studies suggest that completely different pathways are possible in virus assembly and the difference between them depends on the environment.

Acknowledgements

This work was supported by the National Institutes of Health (grants GM 081029, AI090280), by the National Science Foundation (grant 0832651) and was funded in part by the Indiana MetaCyt initiative of Indiana University, through a major grant from the Lilly Endowment, Inc. Partial support from the Center for Hierarchical Manufacturing, CMMI-1025020, is gratefully acknowledged. We are also indebted to Dr Adam Zlotnick for access to his fluorimetry instrumentation.

References

1 S. Casjens, *Virus structure and assembly*, 1985.
2 S. Casjens and J. King, *Annu. Rev. Biochem.*, 1975, **44**, 555–611.
3 J. W. Roberts and J. E. A. Steitz, *Proc. Natl. Acad. Sci. U. S. A.*, 1967, **58**, 1416.
4 E. Hiebert, J. B. Bancroft and C. E. Bracker, *Virology*, 1968, **34**, 492–508.
5 J. A. Speir, S. Munshi, G. J. Wang, T. S. Baker and J. E. Johnson, *Structure*, 1995, **3**, 63–78.
6 D. Caspar and A. Klug, *Cold Spring Harbor Symp. Quant. Biol.*, 1962, **27**, 1–24.
7 A. Y. Morozov, R. Bruinsma and J. Rudnick, *J. Chem. Phys.*, 2009, **131**, 155101.
8 S. Katen and A. Zlotnick, in *Methods in Enzymology*, ed. M. L. Johnson, J. M. Holt and G. K. Ackers, Elsevier Academic Press Inc, San Diego, 2009, vol. 455, 395–417.
9 P. E. Prevelige, D. Thomas and J. King, *Biophys. J.*, 1993, **64**, 824–835.
10 A. Zlotnick, I. Palmer, J. D. Kaufman, S. J. Stahl, A. C. Steven and P. T. Wingfield, *Acta Crystallogr., Sect. D: Biol. Crystallogr.*, 1999, **55**, 717–720.
11 A. Zlotnick, R. Aldrich, J. Johnson, P. Ceres and M. Young, *Virology*, 2000, **277**, 450–456.
12 M. F. Hagan and O. M. Elrad, *Biophys. J.*, 2010, **98**, 1065–1074.
13 A. McPherson, *BioEssays*, 2005, **27**, 447–458.
14 J. B. Bancroft, E. Hiebert and C. E. Bracker, *Virology*, 1969, **39**, 924–930.
15 Y. Hu, R. Zandi, A. Anavitarte, C. M. Knobler and W. M. Gelbart, *Biophys. J.*, 2008, **94**, 1428–1436.
16 M. Comellas-Aragones, H. Engelkamp, V. I. Claessen, N. A. J. M. Sommerdijk, A. E. Rowan, P. C. M. Christianen, J. C. Maan, B. J. M. Verduin, J. J. L. M. Cornelissen and R. J. M. Nolte, *Nat. Nanotechnol.*, 2007, **2**, 635–639.
17 N. L. Goicochea, M. De, V. M. Rotello, S. Mukhopadhyay and B. Dragnea, *Nano Lett.*, 2007, **7**, 2281–2290.
18 L. Loo, R. H. Guenther, S. A. Lommel and S. Franzen, *J. Am. Chem. Soc.*, 2007, **129**, 11111–11117.
19 C. Chen, M. C. Daniel, Z. T. Quinkert, M. De, B. Stein, V. D. Bowman, P. R. Chipman, V. M. Rotello, C. C. Kao and B. Dragnea, *Nano Lett.*, 2006, **6**, 611–615.
20 S. K. Dixit, N. L. Goicochea, M.-C. Daniel, A. Murali, L. Bronstein, M. De, B. Stein, V. M. Rotello, C. C. Kao and B. Dragnea, *Nano Lett.*, 2006, **6**, 1993–1999.
21 X. Huang, L. M. Bronstein, J. Retrum, C. DuFort, I. Tsvetkova, S. Aniagyei, B. Stein, G. Stucky, B. McKenna, N. Remmes, D. Baxter, C. C. Kao and B. Dragnea, *Nano Lett.*, 2007, **7**, 2407–2416.
22 F. Li, K. Li, Z. Q. Cui, Z. P. Zhang, H. P. Wei, D. Gao, J. Y. Deng and X. E. Zhang, *Small*, 2010, **6**, 2301–2308.
23 R. Lucas, S. Larson and A. McPherson, *J. Mol. Biol.*, 2002, **317**, 95–108.
24 J. Sun, C. DuFort, M.-C. Daniel, A. Murali, C. Chen, K. Gopinath, B. Stein, M. De, V. M. Rotello, A. Holzenburg, C. C. Kao and B. Dragnea, *Proc. Natl. Acad. Sci. U. S. A.*, 2007, **104**, 1354–1359.
25 M. F. Hagan, *J. Chem. Phys.*, 2009, **130**, 114902.
26 A. Siber, R. Zandi and R. Podgornik, *Phys. Rev. E: Stat. Nonlinear Soft Matter Phys.*, 2010, 81.
27 M.-C. Daniel, I. B. Tsvetkova, Z. T. Quinkert, A. Murali, M. De, V. M. Rotello, C. C. Kao and B. Dragnea, *ACS Nano*, 2010, **4**, 3853–3860.
28 M. Vieweger, N. Goicochea, E. S. Koh and B. Dragnea, *ACS Nano*, 2011, **5**, 7324–7333.
29 K. W. Adolph and P. J. G. Butler, *J. Mol. Biol.*, 1974, **88**, 327–338.
30 L. Lavelle, M. Gingery, M. Phillips, W. M. Gelbart, C. M. Knobler, R. D. Cadena-Nava, J. R. Vega-Acosta, L. A. Pinedo-Torres and J. Ruiz-Garcia, *J. Phys. Chem. B*, 2009, **113**, 3813–3819.
31 M. Cuillel, C. Berthet-Colominas, P. A. Timmins and M. Zulauf, *Eur. Biophys. J.*, 1987, **15**, 169–176.
32 J. M. Johnson, D. A. Willits, M. J. Young and A. Zlotnick, *J. Mol. Biol.*, 2004, **335**, 455–464.
33 J. R. Lakowicz, *Anal. Biochem.*, 2001, **298**, 1–24.
34 E. Dulkeith, A. C. Morteani, T. Niedereichholz, T. A. Klar, J. Feldmann, S. A. Levi, F. van Veggel, D. N. Reinhoudt, M. Moller and D. I. Gittins, *Phys. Rev. Lett.*, 2002, 89.
35 J. W. Zhao, L. Q. Luo, X. R. Yang, E. K. Wang and S. J. Dong, *Electroanalysis*, 1999, **11**, 1108–1111.
36 J. Pillay, K. I. Ozoemena, R. T. Tshikhudo and R. M. Moutloali, *Langmuir*, 2010, **26**, 9061–9068.
37 G. A. Somorjai and Y. Li, *Introduction to Surface Chemistry and Catalysis*, 2 edn, Wiley, John & Sons, 2010.
38 K. Dill and S. Bromberg, *Molecular Driving Forces: Statistical Thermodynamics in Chemistry and Biology*, Garland Science Publishing Co., New York, 2003.
39 I. M. Klotz, *Ligand-Receptor Energetics* John Wiley and Sons, Inc., New York, 1997.
40 J. M. Johnson, J. H. Tang, Y. Nyame, D. Willits, M. J. Young and A. Zlotnick, *Nano Lett.*, 2005, **5**, 765–770.
41 B. Dragnea, C. Chen, E.-S. Kwak, B. Stein and C. C. Kao, *J. Am. Chem. Soc.*, 2003, **125**, 6374–6375.
42 J. R. Lakowicz, *Principles of Fluorescence Spectroscopy*, Kluwer Academic/Plenum, New York, 1999.